Title: Vertical Graphene Sheets as a Lightweight Light Absorber

Author: Keivan Davami John Cortes Nina Hong Igor Bargatin

PII: S0025-5408(15)30175-6
DOI: http://dx.doi.org/doi:10.1016/j.materresbull.2015.10.041
Reference: MRB 8463

To appear in: *MRB*

Received date: 18-8-2015
Accepted date: 23-10-2015

Please cite this article as: Keivan Davami, John Cortes, Nina Hong, Igor Bargatin, Vertical Graphene Sheets as a Lightweight Light Absorber, Materials Research Bulletin http://dx.doi.org/10.1016/j.materresbull.2015.10.041

Vertical Graphene Sheets as a Lightweight Light Absorber

Keivan Davami[1]*, John Cortes[1], Nina Hong[2], and Igor Bargatin[1*]

[1]Department of Mechanical Engineering and Applied Mechanics, University of Pennsylvania, Philadelphia, PA, USA, 19104

[2] J.A. Woollam Co., Inc., Lincoln, NE, USA, 68508

* Corresponding Authors: *kdavami@seas.upenn.edu, bargatin@seas.upenn.edu*

Highlights:

- A comprehensive study on the optical properties of vertical graphene (VG) sheets on copper (for the first time) and silicon was conducted.
- A new and innovative method was developed to separate the VG sheets from the substrate.
- An index of refraction close to unity in the visible and infrared range as well as a coefficient of absorption higher than those of forests of carbon nanotubes (CNTs) were achieved.
- The specific absorption (absorption divided by the areal density) of VG sheets grown on copper was measured to be two times higher than previously reported results for VG sheets grown on silicon and much higher than that of a CNT forest, showing their potential as a lightweight light absorber.
- The great potential of VG sheets for solar thermal applications was illustrated by presenting the results of the solar reflectance of the VG sheets.

Abstract:

We report the optical properties and solar reflectance of catalyst-free vertical graphene (VG) sheets grown on two types of substrate, copper and silicon, over a wide range of wavelengths and for the first time, a method for the separation of the sheets from the substrate. The index of refraction of the VG sheets was close to unity in the visible and infrared range, while the coefficient of absorption was higher than those of forests of carbon nanotubes (CNTs). A total reflectance (diffuse and specular) of less than 10% was observed for the VG sheets in the visible range. For VG sheets grown on a copper substrate, the specific absorption (absorption divided by the areal density) at a wavelength of 633 nm was measured to be two times higher than previously reported results for VG sheets grown on a silicon substrate and much higher than that of a CNT forest.

KEYWORDS: A. nanostructures, A. thin films, A. surfaces, B. plasma deposition, B. optical properties.

1. Introduction

Creating a black body, a surface that absorbs all incident electromagnetic radiation regardless of frequency or angle of incidence, has been the subject for much research since Kirchhoff introduced the theoretical concept of a perfect black body in 1860. By definition, a black body is a perfect absorber and emitter that radiates at all frequencies with a spectral energy distribution given by Plank's law. Applications of black-body-like objects cut across a variety of topics including energy collectors [1-4], infrared thermal detectors [5-7], radar-absorbent materials for radar invisibility [8], and bolometers [9-10].

Progress in nanotechnology accelerated discovery of materials with exceptional optical characteristics for novel black bodies or antireflection coatings. Adding nanostructures to the surface of an object is a proven method for manipulating the optical properties of the surface and creating antireflective surfaces [11-13]. For example, the reflectivity of a carbon substrate was reduced 10 times in the wavelength range from 0.1 to 4 μm when graphene nanostructures were formed on the surface by etching the substrate [14]. Carbon-based nanostructures such as CNTs [15] and carbon nanowalls (CNWs) [16] have a reflectance much less than that of glassy carbon and were recently heralded as a new approach to creating blackbody-like materials. Theoretical studies of a forest of CNTs indicated an index of refraction close to unity [17], with experimental measurements confirming theoretical predictions and showing negligible transmittance and a total optical reflectance as low as 0.045% in the visible range [18].

Carbon nanowalls (CNWs), also colloquially called vertical graphene (VG) sheets, are nanoscale flakes of 1to ~20 layers of graphene that grow almost vertically on a substrate [19-21]. VG's ease of fabrication and low cost has led to applications in energy storage [22, 23], bio applications [24], and nanocomposites [25]. Optical characterization of VG on Si substrates recently demonstrated excellent light absorption and ultra-low total reflectance of less than 0.13% in the visible range [26]. These optical properties, in combination with catalyst-free growth on a wide range of substrates, make VG sheets an excellent choice for creating blackbody coatings. VG sheets are mechanically robust and do not collapse even if several microns high [27], in contrast to the behavior of multi-walled CNT forests, where bending and collapse has been shown to decrease surface roughness and increase optical reflectivity [28]. In addition, VG

sheets can exhibit spectral selectivity for solar thermal applications, unlike CNT forests which have high absorption from visible to far infrared [29].

While the optical properties of VG sheets have been reported in a few reports previously [16, 26], the results are limited to VG sheets grown on silicon substrates; however, in order to take advantage of these nanostructures as lightweight light absorbers, it is important to be able to grow them on different surfaces readily without any degradation in their optical properties. While VG sheets were previously grown on copper successfully [27], there are no reports on their properties on copper. The grown nanostructures on silicon and copper substrates have different morphologies, and therefore, different properties are expected [27]. Also, in contrast to silicon, copper can be easily deposited through electroless deposition as well as electron-beam or thermal evaporation [30-32]. Here, we report the synthesis and characterization of VG sheets as well as an extensive study of their light absorption and reflection characteristics on both copper and silicon substrates. We present measurements of specular and total reflection as well as the inferred optical constants. Specific absorption of different samples was calculated and compared with results reported before, showing the excellent potential of VG sheets on copper as lightweight light absorbers for the first time. A novel method was also developed to separate VG sheets as a layer from the substrate to facilitate their applications on a wide range of surfaces.

2. Experimental Methods

2.1. Synthesis

A radio-frequency plasma-enhanced chemical vapor deposition (RF-PECVD) method was used to synthesize VG. This method was reported in previous work [27] but a summary is provided here. Two different types of substrates, Cu and Si, were cleaned with acetone and isopropyl alcohol (IPA), rinsed off with water, and dried with N_2 gas. The substrates were placed on the sample stage in a PECVD chamber. The sample stage temperature was raised to 680°C via Joule heating at the pressure of 1 Torr. A mixture of methane and hydrogen was inserted into the

chamber to ignite the plasma. The RF power was set at 900 W. Different deposition times in the range of 10 to 80 min were used. The chamber was then cooled down to room temperature to prevent the oxidation of the sheets, then vented, and the samples were taken out. For clarity, the growth time of each sample is presented after the name of its substrate in the text below. For example, sample Si20 corresponds to VG sheets grown on a Si substrate with a growth time of 20 min. More information about the samples is presented in Table S1 in the Supplementary Information.

2.2. Characterization

A scanning electron microscope (SEM - JEOL 7500 HRSEM) operating at 5.00 kV was used for imaging and studying the morphology of the VG sheets. The structure of the VG sheets was also characterized on a copper grid by using a JEOL JEM 2100 transmission electron microscope (TEM) operating at 200 kV. A non-contact Zygo profilometer was used to study the morphologies and roughness of the samples. Additional information about the structural characterization using Raman spectroscopy is provided in the Sections 2 of the Supplementary Information, respectively.

A variable angle spectroscopic ellipsometer (VASE) from J.A. Woollam Co. was used to obtain the complex refractive indices of the VG sheets in the visible and near infrared regions. The polarization-dependent reflection intensities were measured using a J.A. Woollam M-2000 spectroscopic ellipsometer in the spectral range of 193 nm to 1690 nm. The angle of incidence was varied from 45˚ to 75˚ in 1˚ increments. An Agilent Cary 500E UV-Vis-NIR spectrophotometer equipped with a 150 mm diameter Labsphere Spectralon integrating sphere was used for the total reflectance (R) and transmittance (T) measurements in the ultraviolet, visible and near infrared regions (250 to 2500 nm). For VG sheets on the silicon substrate, both total transmittance and total reflectance were measured. For the VG sheets on copper, only the total reflectance was measured since the transmittance was negligible. An angle of incidence of 7 degrees was used in all cases. A Nicolet 560 FT-IR spectrophotometer equipped with a 102-mm diameter Labsphere Infragold integrating sphere was used for the measurement in the infrared region from 2 to 20 μm. All the samples were scanned three times and the results were averaged.

3. Results and Discussion

Macroscopic images of the samples are shown in Figure 1. The colors of the samples grown on Si substrates, as apparent to the naked eye, ranged from light gray for shorter growth time (~10 min) to completely black for the longer periods. Thick layers of VG sheets on Cu substrates also appeared black, but thinner ones appeared dark green. Optial micsrocope images as well as the surface topography of the samples are shown in Figure 1(c). For the surface topography, a non-contact optical profilometer was used (Figure 1(c), third column). In this method, white light interferometry is applied to obtain the topology of the surface. As expected, for surfaces that are highly absorbent in the visible range, no light was detected and the profilometer was not able to record any images (see image Si80 in Figure 1(c) as a representative of the highly absorbent surfaces, the green areas are scratches). Optical microscope images and surface topography of bare Si and Cu substrates are shown in Section 3 of the Supplementary Information.

Figures 2 (a-d) show the top and cross-sectional views of as-grown VG sheets on Si80 and Cu80 samples. The VG forms a porous coating made of highly curved and randomly oriented sheets with a length of up to a few hundred nanometers. The sheets grow on a thin amorphous carbon and graphitic layer that forms on the substrate at the initial stages of the growth. VG sheets grown on Si and Cu substrates differed from each other in morphology and density (compare Fig. 2a/2b to 2c/2d). Additional images of different samples are shown in Section 4 of the Supplementary Information. The film thickness (height of the sheets) and their areal density increased with the growth time (Figure 1(c) and Table S1) and typically reached 400–500 nm for VG grown for ~80 min on Si and Cu substrates. In literature, growth rates of up to 4.5 μm in 25 min have been reported, achieved by optimization of growth parameters such as methane concentration and the substrate temperature [33, 34]. A detailed comparison of the VG sheets on different substrates and the effect of various growth parameters was presented in Ref. 27.

Figure 3(a,b) show TEMs image of as-grown VG sheets on Cu and Si substrates. Also in Figure 3(a) carbon onions and amorphous carbon that often form during the growth of VG sheets can be observed [35]. The edges of the sheets usually fold upon themselves, making them more rigid. Each VG sheet is composed of one to several carbon layers, with an inter-layer distance measured to be 3.5 Å (Figure 3(b)), consistent with graphite. Typically, the number of the layers is the highest at the base of the sheet and the lowest at the edges, making the sheets tapered [35]. The thickest bottom part of the sheet usually has a thickness in the range of 3 to 5 nm,

corresponding to 10 to 15 layers (Figure 3(b)). While the variation in the numbers of layers makes VG sheets very different from single layer graphene, they are still often referred to as "vertical graphene".

Ellipsometry was used to extract the optical constants of samples with different growth times and on different substrates (Figure 4(a) and (b)). The optical constants, n and k, of the VG coating were modeled using Lorentz oscillators along with a Kramers-Kronig consistent Sellmeier function [36]. In the model, the VG sheets were treated as the effective substrate, i.e., the presence of Si or Cu substrate was ignored, which is a reasonable assumption if the VG sheets are opaque. The pseudo-optical constants of different samples are almost the same at all three test angles (50°, 60°, and 70°), as shown in Section 5 of the Supplementary Information for a representative sample with a growth time of ~20 min (sample Si20).The fact that the pseudo-optical constants are largely independent of the angle of incidence indicates that the samples are sufficiently opaque and the effective substrate approximation is valid.

In the visible wavelength, an index of refraction ranging from 1.03 to 1.32 was observed for the sample Si80, which had the longest growth time and a thickness of ~500 nm (Figure 4(a)). This is smaller than the previously reported refractive index of 1.27-1.42 for a 0.36 μm-thick CNT coating in the wavelength range of 300-2200 nm [29]. The index of refraction for Si20 and Si40 was ~1.5 which is in good agreement with the previously reported results from 1.2 to 1.5 [37]. For Cu80 the index of refraction was measured to be in the range from 1.00 to 1.28 for wavelengths from 450 nm to 1100 nm. For comparison, Figure 4 also shows the index of refraction for graphite from Ref.38, which varies from ~2.7 to ~3.2.

The near-unity index of refraction for Si20, Si40, Cu80, and Si80 is attributed to the sparseness of VG sheets. When the volumetric density of the material goes down, electron density and permittivity decline too [15], which in turn provides better impedance matching to air and suppresses the reflection [29]. A gradient in the index of refraction of VG sheets was reported in Refs. [16, 26], where it gradually increased from ~1 at the top to ~2 at the bottom of the sheets with a height of ~800 nm. This was attributed to the higher amount of graphitic and amorphous carbon at the bottom of the sheets as well as thicker bases of VG sheets compared to their tops (Figure 5). The index of refraction for such a coating at each cross section, $n_{eff}(z)$, can be estimated by averaging the index of refraction of the ambient medium (here air), n_a, and the bulk

material (here, amorphous carbon and graphite), n_m, weighted by the quantity of material present at the corresponding depth (Figure. 5) [11]. Thus, according to the weighting formula [39]:

$$n_{eff}(z) = f_{bulk}(z)n_m + (1 - f_{bulk}(z))n_{air} \quad (1)$$

Where $f_{bulk}(z)$ is the bulk material fraction at the depth z. It should be noted that this relation is valid as long as the spacing of the flakes, d, are much smaller than the wavelength (Figure 5). Considering that there is an increase in the cross section of the sheets from their top to base, we expect the index of refraction profile to exhibit the general shape shown in Figure 5.

If each sheet is assumed as a multilayer coating similar to the schematic in Figure 5, the index of refraction would increase in each subsequent layer ($n_i < n_{i-1}$) without sudden jumps. When the index of refraction at the top interface (top of the sheets), n_1, is approximately equal to the index of refraction of the ambient media, n_a, light proceeds into the film with minimal reflection at this outer interface. The total reflectance is a sum of partial reflections from multiple segments with diverse index of refractions (n_1, n_2, ..,n_l), coming from different depths, z, with different phase shifts. If the gradual change of index occurs over an optical distance comparable with the wavelength, destructive interference will cause a significant suppression of reflectance [11]. Thus, the morphology of VG sheets affects their optical properties by weakening the reflection at the interface [40, 41].

A critical parameter to evaluate the potential of the VG sheets as a lightweight light absorbent coating is the coefficient of absorption, $\alpha = \frac{4\pi k}{\lambda}$, where k is the index of extinction, and λ is the wavelength. Figure 6 shows α for VG sheets on Si substrates with different thicknesses as well as Cu80. For comparison, also shown is the absorption coefficient of gallium arsenide (GaAs) [42]. GaAs is a direct bandgap semiconductor (1.42 eV) and for wavelengths below the bandgap edge (~850 nm), GaAs is an efficient light absorber that is frequently used in thin-film solar cells and light-emission devices [43, 44]. It can be seen that the VG sheets have a bigger α compared to GaAs in the visible range, despite the fact that VG sheets are less dense than bulk GaAs.

The relatively larger coefficient of absorption of VG sheets is attributed to the small bandgap of graphene sheets. It is known that the zero band gap and vanishing density of states at the Fermi level give the single-layer graphene its semimetal properties. However, that is not the case for VG sheets due to the edge and surface effect [45]: a range of bandgaps from 0.2 to 0.8 eV were reported for VG [37]. Due to the small band gap of the VG sheets, a wide range of photons have energy higher than the bandgap and a significant number of electrons can interact with the photons, become excited, and result in the absorption of the photons. According to the calculated absorption coefficient, the absorption length ($1/\alpha$) is less than 100 nm for VG sheets grown for 20 min or longer, which is significantly smaller than the absorption length of 8.3 μm measured for 300 μm-thick CNT forests [18]. This shows that the complete absorption of light can be obtained with a much thinner coating (shorter VG sheets) than for CNTs.

The reflection intensities of p- and s-polarized light upon VG sheets were measured to evaluate polarization-dependent specular reflection. Figure 7 shows the reflection intensity versus the angle of incidence (45° to 75° with 1° intervals) for sample Si80 and at a wavelength of 633 nm for different polarizations. The reflection intensity is higher in larger angles of incidence and for s-polarized light in comparison with p-polarized. When the material is completely transparent, the reflection intensity of p-polarized light, R(p), vanishes at the Brewster's angle. However, since the VG sheets are efficient light absorbers, the index of extinction does not vanish completely, and instead R(p) reaches a minimum at the pseudo-Brewster's angle [46]. For the sample in Figure 7, the pseudo-Brewster's angle is 55°.

The total reflectance for different samples in the UV-Vis-NIR is shown in Figure 8(a). The transmittance of the Si80 sample is also shown in this figure and is almost indistinguishable from zero. The reflectance of the four samples generally rises with the wavelength. The thicker samples have a smaller reflectance (compare Cu10 and Cu80); however, at some wavelengths (650 nm to 850 nm) the thinnest and the least opaque sample, Cu10, shows a very small reflectivity too that is attributed to interference effects. Si80 has the minimum total reflectance in the visible range with a value of 3.5%, similar to that reported before for CNWs on Si substrates [16]. Cu80 and Cu20 have reflectance below 15% and 22% in the visible range, respectively.

Figure 8(b) shows the reflectance in the IR region. The reflectance of samples Si80, Cu10, and Cu20 abruptly increases with an increase in the wavelength. Interestingly, the reflectance of

sample Cu80 is almost constant at wavelengths from ~2 μm to ~6 μm and only after that escalates with a sharp slope. The overlapping of the results in the wavelength range of 2.0 to 2.5 μm in Fig 8(a) and (b) validates the accuracy of the measurements.

The low reflectance of samples Si80 and Cu80 is attributed to two main characteristics. The first is the high absorption due to the abundance of edges that affect the electronic structure of the sheets [26, 16], and second, an index of refraction close to unity at the interface that results in a small reflectance at the coating-air interface. The large quantity of edges in the Si80 is attributed to the secondary nucleation and growth of the small VG sheets on the surface of the bigger VG sheets, and in Cu80, is due to the growth of the dense and small VG sheets (Figure 2(a-d)). The slightly higher absorption of sample Si80 compared to Cu80 can be attributed to the existence of the secondary grown VG sheets that make Si80 ~4 times denser than Cu80 (see Table S1 in the Supplementary Information). These extra spikes heighten the surface corrugation and enhance diffuse scattering [18]. Also, the VG sheets on Si80 had a wider range of tilt angles and surface areas that accommodate incident light with various angles of incidence (compare Figure 2(b) and 2(d)).

According to the law of conservation of energy, reflectivity, transmissivity, and absorptivity add up to unity in thermal equilibrium. Considering that the transmissivity for the samples is zero, the absorptivity was calculated from 1-reflectivity. Figure 8(c) compares the absorptivity of different samples. As can be seen here, for sample Si80 and sample Cu80 the absorptivity is above 90% in the visible range. The absorptivity of sample Si80 reaches ~97% in the visible range. Since the emissivity of an object equals its absorptivity according to Kirchhoff's law, it can be concluded that the emissivity of VG sheets in the visible range is close to that of an ideal black body object.

The results of the optical measurements in Figure 8 demonstrate that VG coatings are a good choice for solar thermal energy applications. A perfect solar thermal coating is a perfect black body in the visible range but has a very low emissivity in the thermal IR region [47]. The solar reflectance (SR), which indicates how much of the typical solar spectrum would be reflected (i.e. not absorbed), was calculated for different VG samples by averaging solar spectral reflectance in the wavelength from 250 nm to 2500 nm weighted with air mass 1.5 solar spectral irradiance [48]. The closer SR number is to zero, the better the material absorbs solar radiation. The solar

reflectance of Si80 was the lowest at 0.070 and the samples Cu80, Cu20, and Cu10 followed at 0.139, 0.159, and 0.195, respectively. At the same time, the reflectivity in the thermal infrared region (5 - 15 μm) ranged from 70% to almost 100% for different samples (Fig. 8b), implying very low emissivity. The emissivity and reflectance of the samples at 10 μm at a temperature of 298 K are presented in Table S1 in the Supplementary Information section for comparison.

Considering the high absorption and small areal density of VG sheets on Cu substrates, i.e. a density of ~0.6 g/m^2 for Cu80, these nanostructures can be used as a lightweight absorbent coating material for many applications. Figure 9 compares the optical density (coefficient of absorption multiplied by the thickness) versus areal density of different samples in this study as well as literature-based values for CNTs [18] and several bulk materials [38, 49]. It can be seen that the ~100-nm-thick VG sheet Si20 has an optical density almost equal to that of the 10-μm-thick CNTs [18] but with a much lower areal density. Also, at the same areal density, Si80 and Cu80 surpass the optical density of bulk GaAs and amorphous carbon but they have a smaller optical density when compared with graphite. The specific absorption (absorptivity/areal mass density) of different samples in the visible range was also compared with that of previously reported CNWs on Si substrates [26] as well as a CNT forest [15, 18] and the results are presented in Table S1 in the Supplementary Information section. VG sheets on Cu have an almost two times greater specific absorption compared to previously reported VG sheets grown on Si substrates, and ~22 times larger specific absorption than CNTs. The VG sheets can be grown on a surface or applied as a layer that weighs less than one gram per square meter on top of a surface for complete absorption of visible light (Figure 10). A method for separating the layer of VG sheets from a substrate is presented in Section 6 of the Supplementary Information. Optical property characterization of the separated layer of VG sheets is in progress.

Conclusion

VG sheets were synthesized using an RF-PECVD method. The structural and optical properties of VG sheets with various morphologies on two different types of substrates, silicon and copper, were characterized. An index of refraction close to unity at the surface of the coating was

measured in the visible range that gradually increased with the wavelength. A model based on the multilayer index-gradient antireflection coatings was used to explain the low reflectance of the VG sheets. It was shown that, in the visible range, the light reflectance and transmittance is low in these nanostructures while the light absorption can reach 97%. The absorption coefficient, optical density, and specific absorption (per unit areal mass) were compared for different samples and with previously reported results for a CNT forest as well as VG sheets on Si. It was concluded that VG sheets on copper have the highest specific absorption and are excellent lightweight light absorbers. The easier methods for deposition of copper compared to silicon and superior light absorption at a lower areal density makes VG sheets grown on copper interesting for a wide range of uses. Also, for the first time, a method was developed to separate VG sheets from a substrate. This technique widens the range of potential applications of VG sheets since they can easily be applied on other surfaces, regardless of the type of underlying surface.

Acknowledgements

TEM imaging and analysis by Dr. Hessam Ghassemi are acknowledged. We thank Dr. Michael Ray Jacobson of the Optical Data Associated for his help with the optical characterization and analysis.

References

1. Nunes, C.; Teixeira, V.; Collares-Pereira, M.; Monteiro, A.; Roman, E.; Martin-Gago, J. Deposition of PVD solar absorber coatings for high-efficiency thermal collectors. *Vacuum* **2002**, 67, 623-627.
2. Cao, A.; Zhang, X.; Cailu, X. u.; Wei, B.; Dehai, W. u. Tandem structure of aligned carbon nanotubes on Au and its solar thermal absorption. *Sol. Energy Mater. Sol. Cells* **2002**, 70, 481-486.
3. Lira-Cantú, M.; Sabio, A. M.; Brustenga, A.; Gómez-Romero, P. Electrochemical deposition of black nickel solar absorber coatings on stainless steel AISI316L for thermal solar cells. *Sol. Energy Mater. Sol. Cells.* **2005**, 87, 685-694.
4. Shashikala, A. R.; Sharma, A. K.; Bhandari, D. R. Solar selective black nickel–cobalt coatings on aluminum alloys. *Sol. Energy Mater. Sol. Cells.* **2007,** 91, 629-635.
5. Lehman, J.; Theocharous, E.; Eppeldauer, G.; Pannell, C. Gold-black coatings for freestanding pyroelectric detectors. *Meas. Sci. Technol.* **2003**, 14, 916.
6. Theocharous, E.; Lehman, J. The evaluation of a pyroelectric detector with and without a sprayed multi-walled carbon nanotube coating. *Infrared Phys. Technol.* **2012**, 55, 161-165.
7. Mellouki, I.; Bennaji, N.; Yacoubi, N. IR characterization of graphite black-coating for cryogenic detectors. *Infrared Phys. Technol.* **2007**, 50, 58-62.
8. Folgueras, L. C; Alves, M. A.; Rezende, M. C. Evaluation of a nanostructured microwave absorbent coating applied to a glass fiber/polyphenylene sulfide laminated composite. *Materials Research* **2014**, 17, 197-202.
9. Mahjouri-Samani, M.; Zhou, Y. S.; He, X. N.; Xiong, W.; Hilger, P.; Lu, Y. F. Plasmonic-enhanced carbon nanotube infrared bolometers. *Nanotechnol.* **2013**, 24, 035502.
10. Yan, J.; Kim, M. H.; Elle, J. A.; Sushkov, A. B.; Jenkins, G. S.; Milchberg, H. M.; Fuhrer, M., S.; Drew, H. D. Dual-gated bilayer graphene hot-electron bolometer. *Nat. Nano.***2012**, 7, 472-478.
11. Wilson S.J.; Hutley M.C. The Optical Properties of 'Moth Eye' Antireflection Surfaces. *Optica Acta: International Journal of Optics* **1982**, 29, 993-1009.

12. Huang, Y.-F.; Jen, Y.-J.; Chen, L.-C.; Chen, K.-H.; Chattopadhyay, S. Design for Approaching Cicada-Wing Reflectance in Low- and High-Index Biomimetic Nanostructures. *ACS Nano* **2015**, 9, 301-311.
13. Lee, J. W.; Ye, B. U.; Kim, D.-y.; Kim, J. K.; Heo, J.; Jeong, H. Y.; Kim, M. H.; Choi, W. J.; Baik, J. M. ZnO Nanowire-Based Antireflective Coatings with Double-Nanotextured Surfaces. *ACS Appl. Mater. Interfaces* **2014**, 6, 1375-1379.
14. Matsumoto, T.; Koizumi, T.; Kawakami, Y.; Okamoto, K.; Tomita, M. Perfect blackbody radiation from a graphene nanostructure with application to high-temperature spectral emissivity measurements. *Opt. Express* **2013**, 21, 30964-30974.
15. Mizuno, K.; Ishii, J.; Kishida, H.; Hayamizu, Y.; Yasuda, S.; Futaba, D. N.; Yumura, M.; Hata, K. A black body absorber from vertically aligned single-walled carbon nanotubes. *Proceedings of the National Academy of Sciences* **2009,** 106, 6044-6047.
16. Evlashin, S.; Svyakhovskiy, S.; Suetin, N.; Pilevsky, A.; Murzina, T.; Novikova, N.; Stepanov, A.; Egorov, A.; Rakhimov, A., Optical and IR absorption of multilayer carbon nanowalls. *Carbon* **2014**, 70, 111-118.
17. Bao, H.; Ruan, X.; Fisher, T. S. Optical properties of ordered vertical arrays of multi-walled carbon nanotubes from FDTD simulations. *Opt. Express* **2010**, 18, 6347-6359.
18. Yang, Z. P.; Ci, L.; Bur, J. A.; Lin, S. Y.; Ajayan, P. M. Experimental Observation of an Extremely Dark Material Made By a Low-Density Nanotube Array. *Nano Lett.* **2008**, 8, 446-451.
19. Malesevic, A.; Vitchev, R.; Schouteden, K.; Volodin, A.; Zhang, L.; Tendeloo, G. V.; Vanhulsel, A.; Haesendonck, C. V. Synthesis of few-layer graphene via microwave plasma-enhanced chemical vapour deposition. *Nanotechnol.* **2008**, 19, 305604.
20. Fang, J.; Levchenko, I.; Laan, T. v. d.; Kumar, S.; Ostrikov, K. Multipurpose nanoporous alumina–carbon nanowall bi-dimensional nano-hybrid platform via catalyzed and catalyst-free plasma CVD. *Carbon* **2014**, 78, 627-632.
21. Quinlan, R. A.; Cai, M.; Outlaw, R. A.; Butler, S. M.; Miller, J. R.; Mansour, A. N. Investigation of defects generated in vertically oriented graphene. *Carbon* **2013**, 64, 92-100.

22. Hassan, S.; Suzuki, M.; Mori, S.; El-Moneim, A. A. MnO2/carbon nanowall electrode for future energy storage application: effect of carbon nanowall growth period and MnO_2 mass loading. *RSC Adv.***2014**, 4, 20479-20488.
23. McClure, J. P.; Thornton, J. D.; Jiang, R.; Chu, D.; Cuomo, J. J.; Fedkiw, P. S. Oxygen Reduction on Metal-Free Nitrogen-Doped Carbon Nanowall Electrodes. *J. Electrochem. Soc.* **2012**, 159, F733-F742.
24. Stancu, E. C.; Stanciuc, A.-M.; Vizireanu, S.; Luculescu, C.; Moldovan, L.; Achour, A.; Dinescu, G. Plasma functionalization of carbon nanowalls and its effect on attachment of fibroblast-like cells. *J. Phys. D: Appl. Phys.* **2014**, 47, 265203.
25. Davami, K.; Shaygan, M.; Bargatin, I. Fabrication of vertical graphene-based nanocomposite thin films. *J. Mater. Res.* **2015**, 30, 617-625.
26. Krivchenko, V. A.; Evlashin, S. A.; Mironovich, K. V.; Verbitskiy, N. I.; Nefedov, A.; Wöll, C.; Kozmenkova, A. Y.; Suetin, N. V.; Svyakhovskiy, S. E.; Vyalikh, D. V.; Rakhimov, A. T.; Egorov, A. V.; Yashina, L. V. Carbon nanowalls: the next step for physical manifestation of the black body coating. *Sci. Rep.***2013,** 3.
27. Davami, K.; Shaygan, M.; Kheirabi, N.; Zhao, J.; Kovalenko, D. A.; Rümmeli, M. H.; Opitz, J.; Cuniberti, G.; Lee, J.-S.; Meyyappan, M. Synthesis and characterization of carbon nanowalls on different substrates by radio frequency plasma enhanced chemical vapor deposition. *Carbon* **2014**, 72, 372-380.
28. Mukherjee, S.; Misra, A. Broadband wavelength-selective reflectance and selective polarization by a tip-bent vertically aligned multi-walled carbon nanotube forest. *J. Phys. D: Appl. Phys.* **2014**, 47, 235501.
29. Selvakumar, N.; Krupanidhi, S. B.; Barshilia, H. C. Carbon Nanotube-Based Tandem Absorber with Tunable Spectral Selectivity: Transition from Near-Perfect Blackbody Absorber to Solar Selective Absorber. *J. Adv. Mater.* **2014**, 26, 2552-2557.
30. Scudiero, L.; Fasasi, A.; Griffiths, P. R., Characterization of a controlled electroless deposition of copper thin film on germanium and silicon surfaces. *Appl. Surf. Sci.* **2011,** 257, (9), 4422-4427.
31. Jeon, I.-D.; Barnes, M. C.; Kim, D.-Y.; Hwang, N. M., Origin of positive charging of nanometer-sized clusters generated during thermal evaporation of copper. *J. Cryst. Growth* **2003,** 247, (3–4), 623-630.

32. Yeganeh, M.; Saremi, M., Deposition of thin film copper nanostructures by electron beam physical vapor deposition technique on SiO_2/p-type Si(100) and study of its oxidation behavior. *Int. J. Mod. Phys. B* **2011,** 25, (19), 2567-2574.
33. Mironovich, K. V.; Itkis, D. M.; Semenenko, D. A.; Dagesian, S. A.; Yashina, L. V.; Kataev, E. Y.; Mankelevich, Y. A.; Suetin, N. V.; Krivchenko, V. A. Tailoring of the carbon nanowall microstructure by sharp variation of plasma radical composition. *Phys. Chem. Chem. Phys.***2014**, 16, 25621-25627.
34. Wang, J.; Zhu, M.; Outlaw, R. A.; Zhao, X.; Manos, D. M.; Holloway, B. C. Synthesis of carbon nanosheets by inductively coupled radio-frequency plasma enhanced chemical vapor deposition. *Carbon* **2004**, 42, 2867-2872.
35. Zhao, J.; Shaygan, M.; Eckert, J.; Meyyappan, M.; Rümmeli, M. H. A Growth Mechanism for Free-Standing Vertical Graphene. *Nano Lett.* **2014**, 14, 3064-3071.
36. Roessler, D. M. Kramers-Kronig analysis of reflection data. *Br. J. Appl. Phys.***1965**, 16, 1119.
37. Kawai, S.; Kondo, S.; Takeuchi, W.; Kondo, H.; Hiramatsu, M.; Hori, M. Optical properties of evolutionary grown layers of carbon nanowalls analyzed by spectroscopic ellipsometry. *Jpn. J. Appl. Phys.***2010**, 49, 060220.
38. Djurišić, A. B.; Li, E. H.; Optical properties of graphite. *J. Appl. Phys.* **1999**, 85, 7404-7410.
39. Stavenga, D. G.; Foletti, S.; Palasantzas, G.; Arikawa, K. *Proc. R. Soc. London, Ser. B* **2006**, *273*, 661.
40. Poitras, D.; Dobrowolski, J. A. Toward perfect antireflection coatings. 2. Theory. *Appl. Opt.* **2004**, 43, 1286-1295.
41. Dobrowolski, J. A.; Poitras, D.; Penghui, M. a.; Vakil, H.; Acree, M. Toward perfect antireflection coatings: numerical investigation. *Appl. Opt.* **2002**, 41, 3075-3083.
42. Skauli, T.; Kuo, P. S.; Vodopyanov, K. L.; Pinguet, T. J.; Levi, O.; Eyres, L. A.; Harris, J. S.; Fejer, M. M.; Gerard, B.; Becouarn, L.; Lallier, E. Improved dispersion relations for GaAs and applications to nonlinear optics. *J. Appl. Phys.* **2003**, 94, 6447-6455.
43. Sathasivam, S.; Arnepalli, R. R.; Singh, K. K.; Visser, R. J.; Blackman, C. S.; Carmalt, C. J., A solution based route to GaAs thin films from $As(NMe_2)_3$ and $GaMe_3$ for solar cells. *RSC Adv.* **2015**, 5, 11812-11817.

44. Sheng, X.; Yun, M. H.; Zhang, C.; Al-Okaily, A. M.; Masouraki, M.; Shen, L.; Wang, S.; Wilson, W. L.; Kim, J. Y.; Ferreira, P.; Li, X.; Yablonovitch, E.; Rogers, J. A. Device Architectures for Enhanced Photon Recycling in Thin-Film Multijunction Solar Cells. *Adv. Energy Mater.* **2015**, 5, 1400919.
45. Wu, Y.; Yang, B.; Zong, B.; Sun, H.; Shen, Z.; Feng, Y. Carbon nanowalls and related materials. *J. Mater. Chem.* **2004**, 14, 469-477.
46. Meng, F.-S.; Lin, Y.-H.; Lin, G. R. Omnidirectional reflectance and vanishing Brewster angle of disordered semiconductor nanopillar surface with gradually changed refractive index. *J. Appl. Phys.* **2011**, 109, 083523.
47. Seraphin, B. O. *Solar Energy Conversion – Solid-State Physics Aspects: Topics in Applied Physics* Vol. 31, Springer, Berlin 1979.
48. Levinson, R.; Akbari, H.; Berdahl, P. Measuring solar reflectance—Part II: Review of practical methods. *Solar Energy* **2010**, 84, 1745-1759.
49. Hagemann, H.-J.; Gudat, W.; Kunz, C. Optical constants from the far infrared to the x-ray region: Mg, Al, Cu, Ag, Au, Bi, C, and A12O3. *J. Opt. Soc. Am.***1975**, 65, 742-744.

Figure Captions

Figure 1. *Normal (a) and oblique (b) views of the samples on silicon and copper substrates. (c) From left to right: photographs, optical microscopy, surface topography (using a Zygonon-contact optical profilometer), as well as cross-sectional and top view SEM images of the samples. The scale bar in all the pictures is 100 nm.*

Figure 2. *SEM images of the VG sheets on different substrates. A top view (a), and cross-sectional view (b), of VG sheets grown for 80 min on a Si substrate. A top view (c), and cross-sectional view (d), of VG grown for 80 min on a Cu substrate. In (b) and (d) the tilt angle is 90°.*

Figure 3. *(a) A TEM image of a single sheet and amorphous carbon grown on a Cu substrate, (b) a high magnification TEM image of VG grown on a Si substrate, with inset showing distance between carbon layers.*

Figure 4. *(a) Index of refraction, n, and (b) extinction coefficient, k, of different samples obtained from ellipsometry measurements.*

Figure 5. *A schematic of VG sheets (middle) and the expected index of refraction profile (left). Cross sections A, B, and C are shown on the right as an example.*

Figure 6. *Coefficient of absorption for VG sheets as well as GaAs.*

Figure 7. *Reflection intensity versus the angle of incidence for sample Si80 at a wavelength of 633 nm.*

Figure 8. *Total transmission and reflectance of the samples in the UV-Vis-IR region (a) and in the IR region (b). Calculated absorption from different samples (c).*

Figure 9. *A comparison of the optical density of the samples in this study with those calculated for previously reported CNTs and other bulk materials. The absorption was compared at 650 nm at all the data points.*

Figure 10. *A layer of VG sheets after separation from the substrate (a), a picture showing the flexibility of a layer of VG sheets (b).*

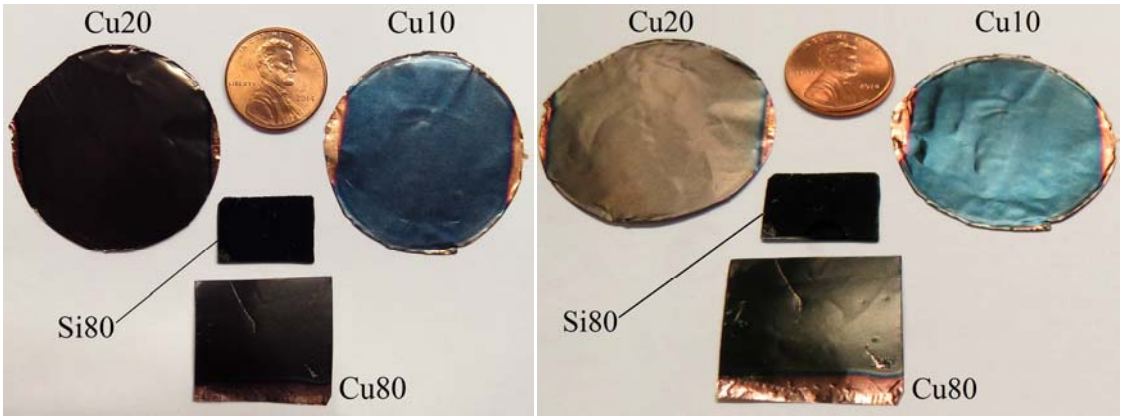

(a) (b)

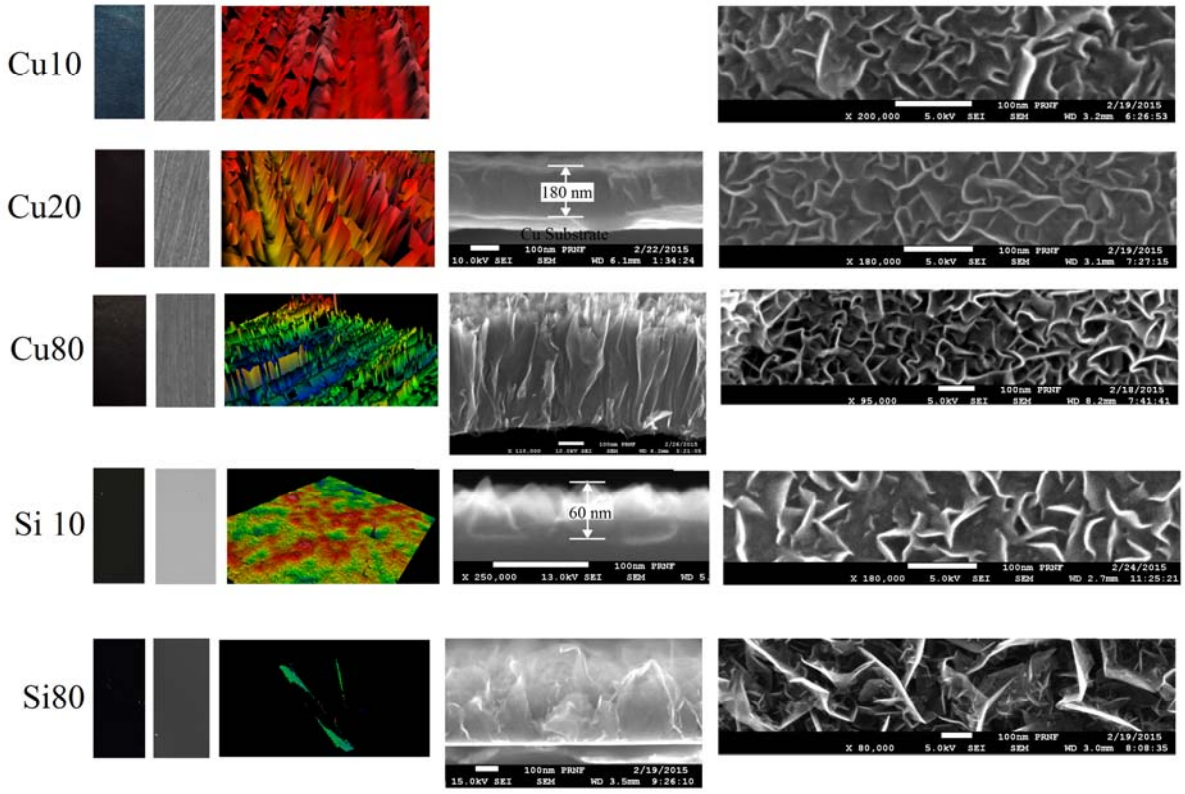

(c)

Figure 1

.

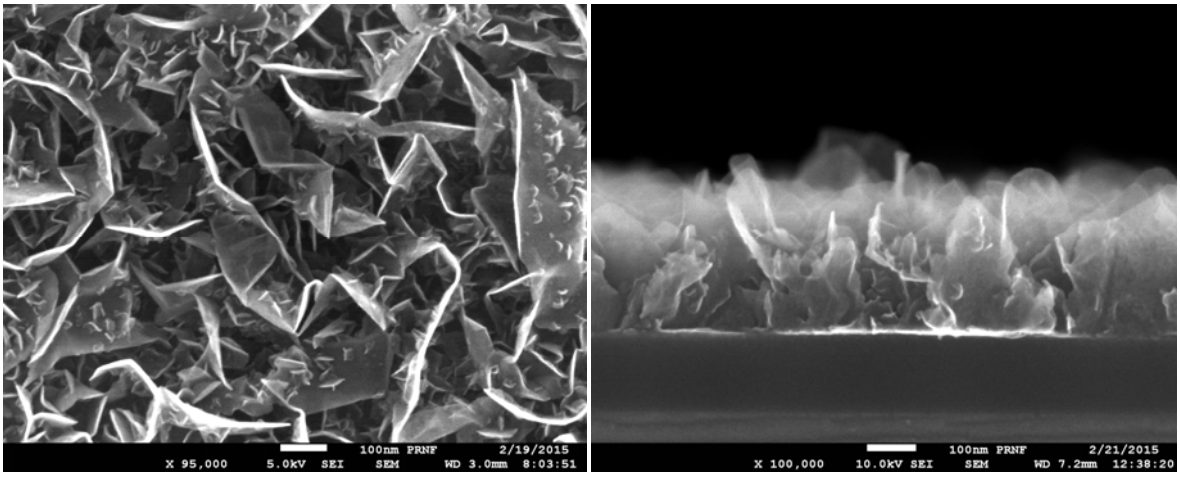

(a) (b)

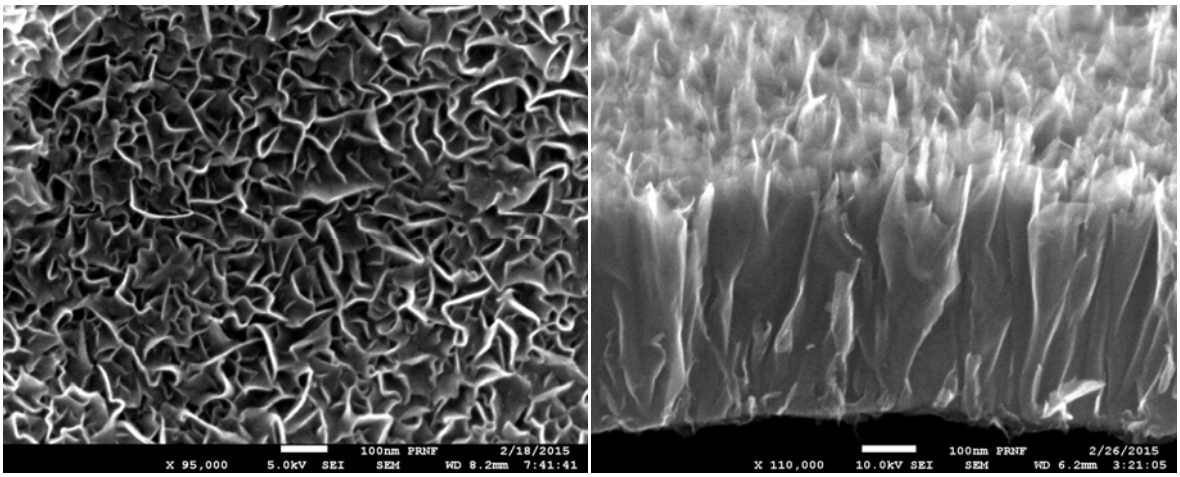

(c) (d)

Figure 2

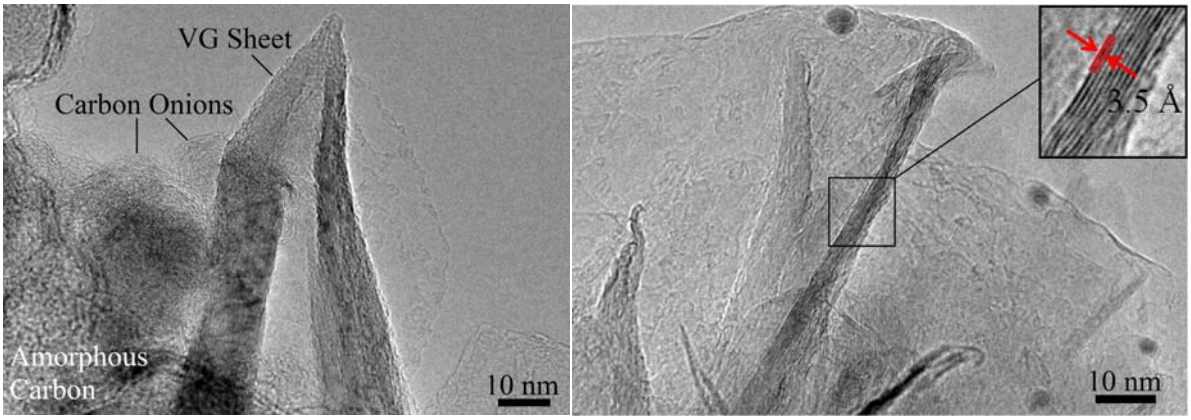

(a) (b)

Figure 3

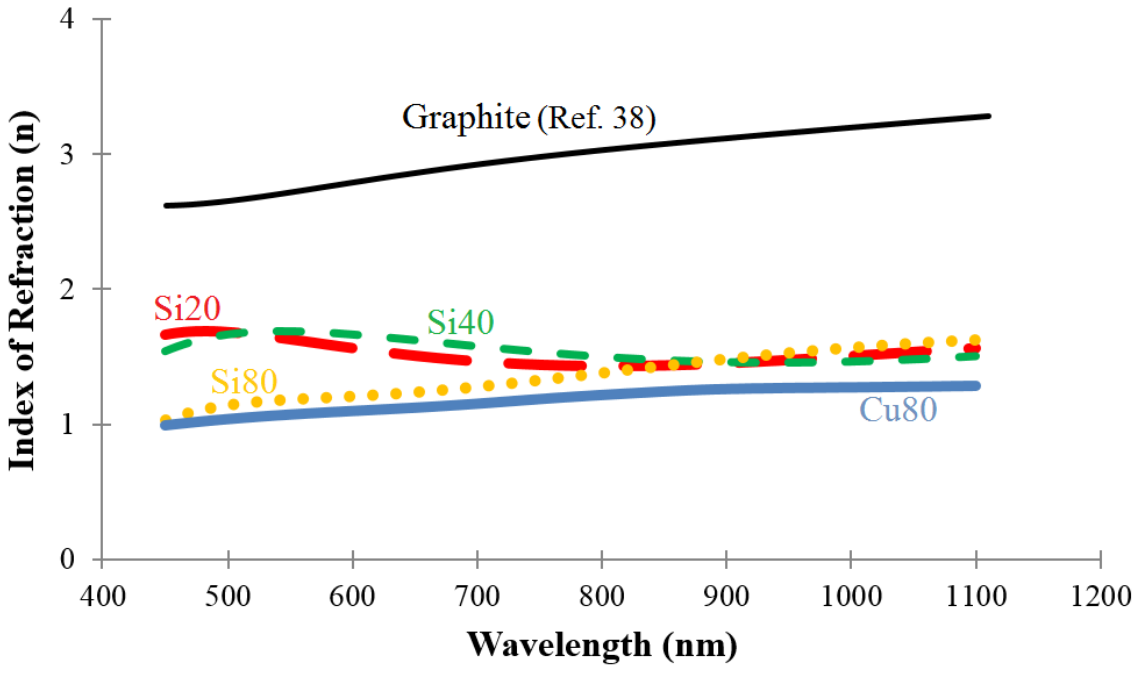

(a)

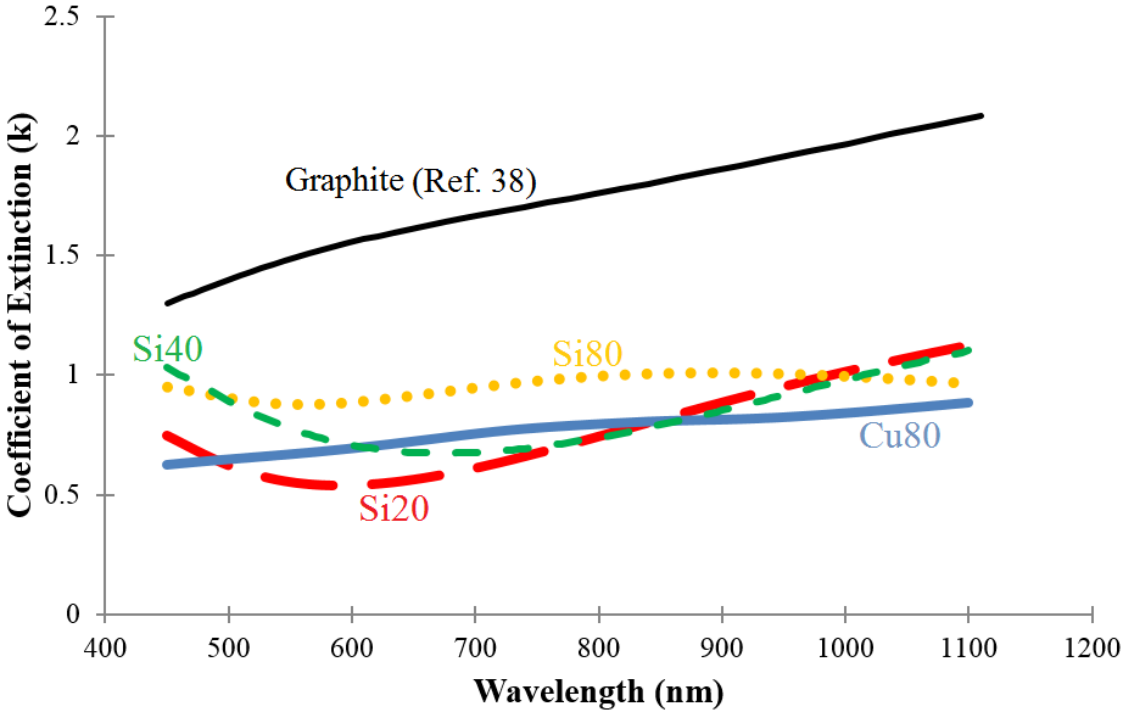

(b)

Figure 4

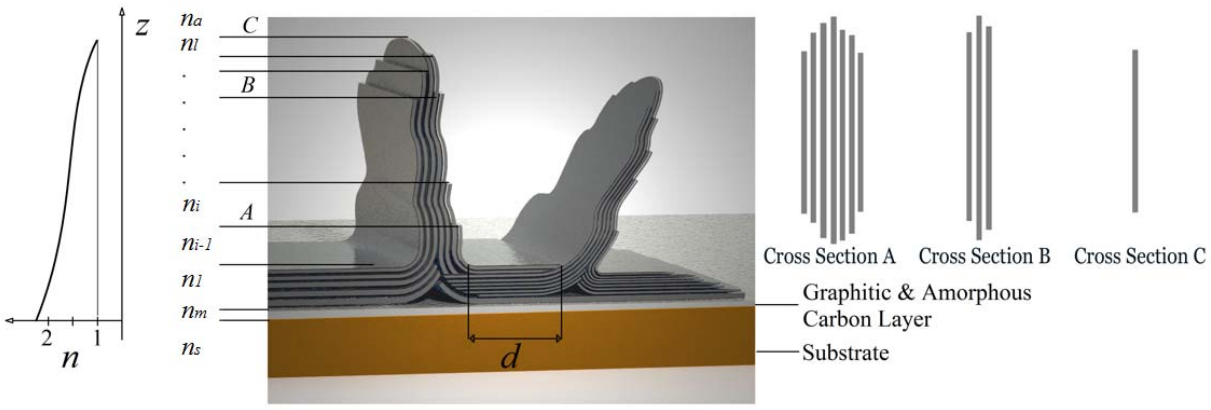

Figure 5

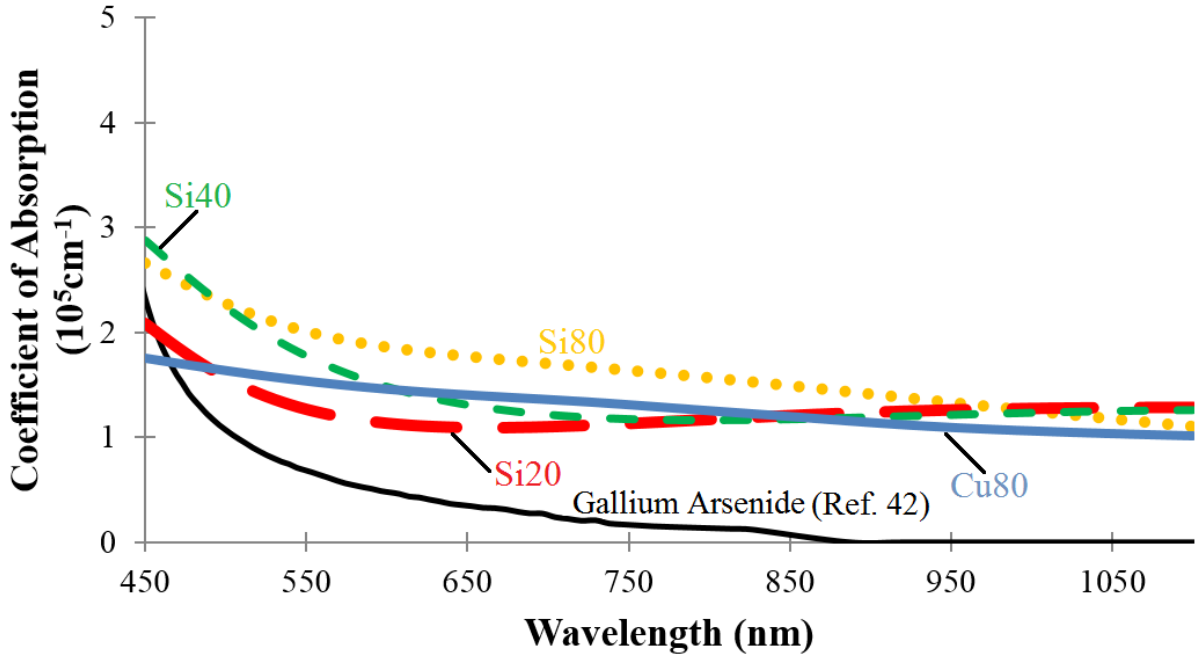

Figure 6

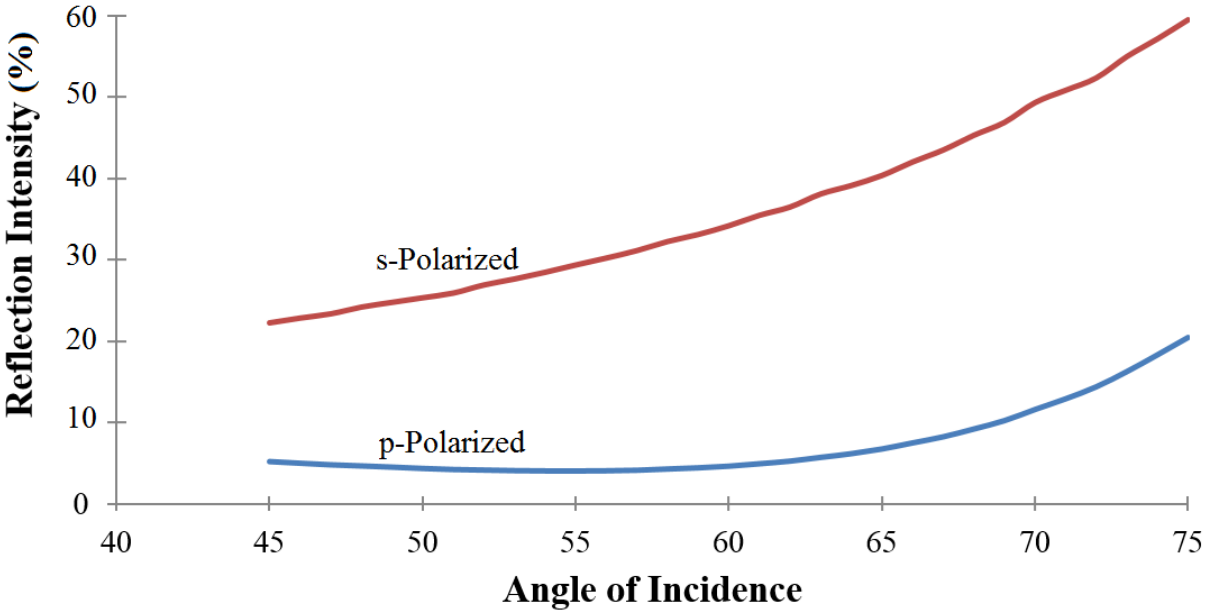

Figure 7

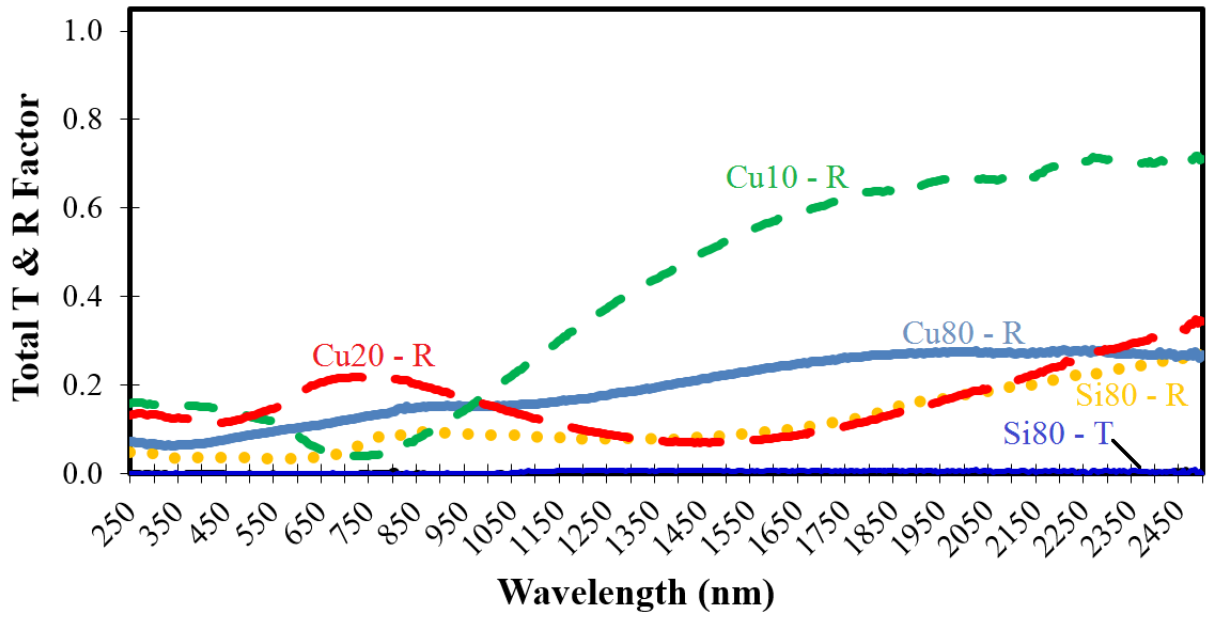

(a)

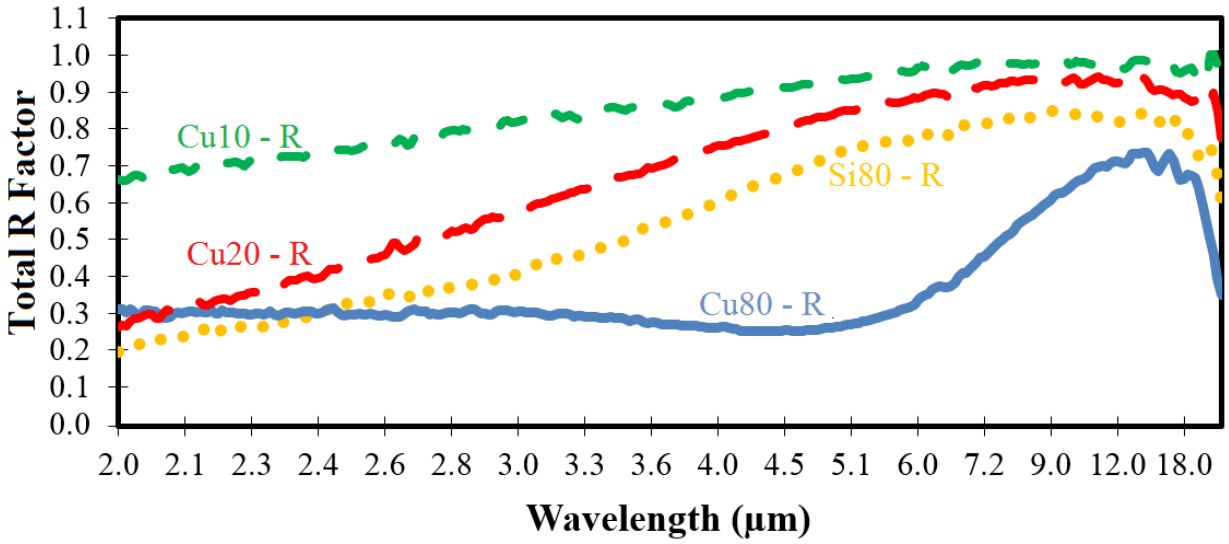

(b)

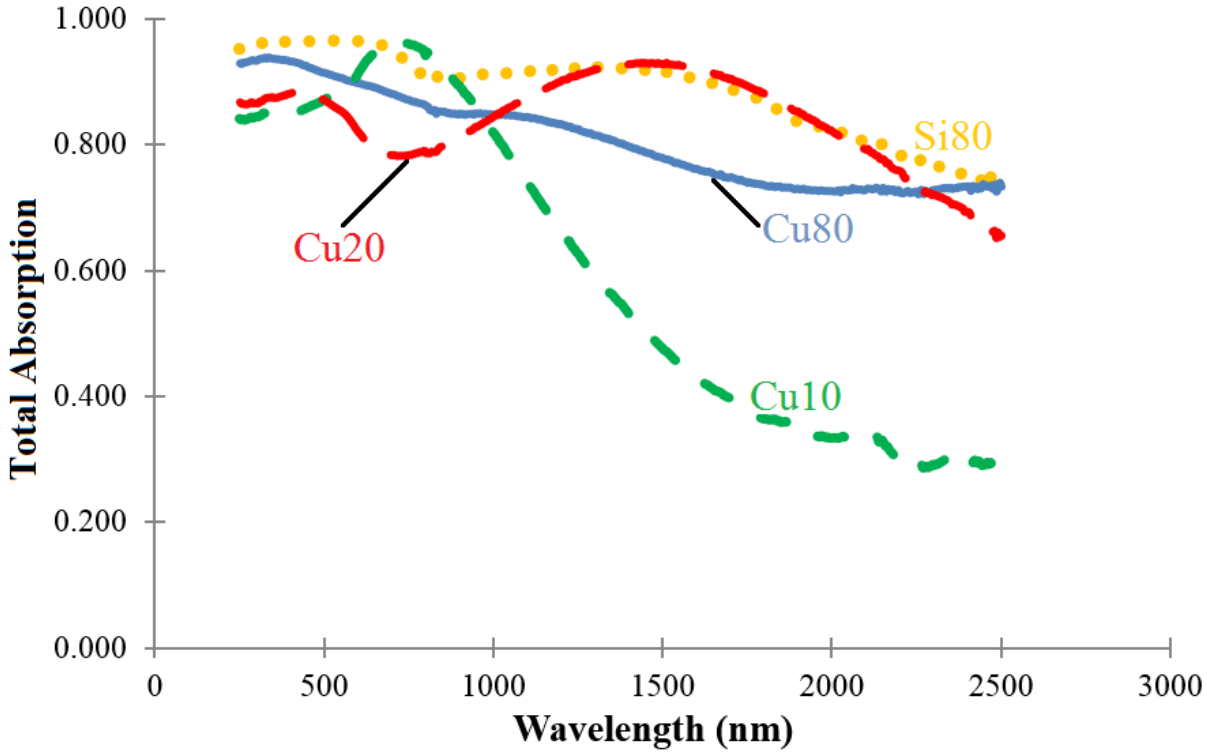

(c)

Figure 8

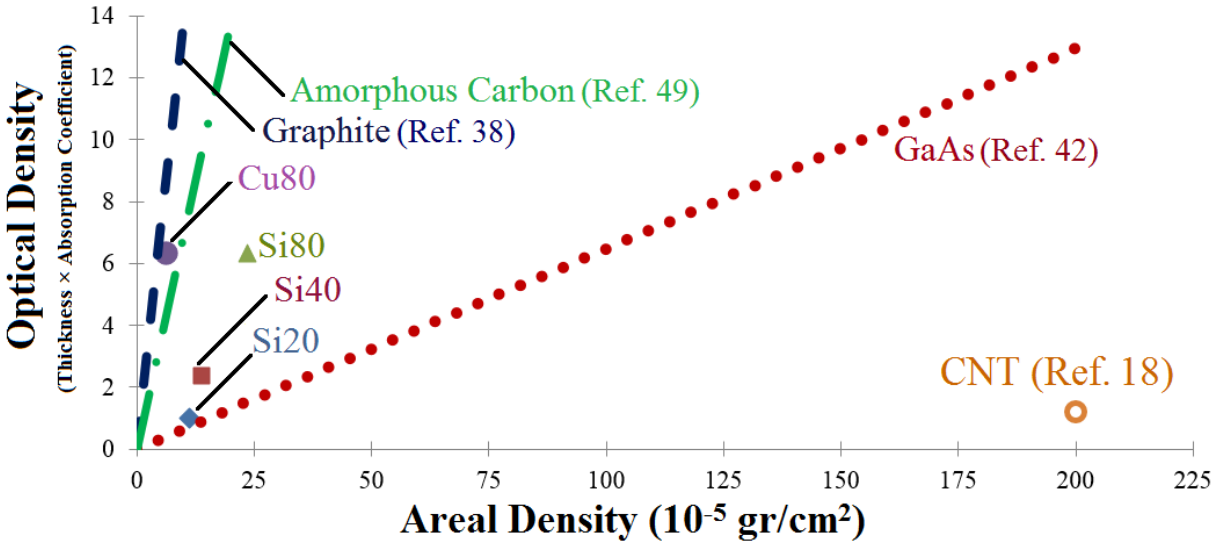

Figure 9

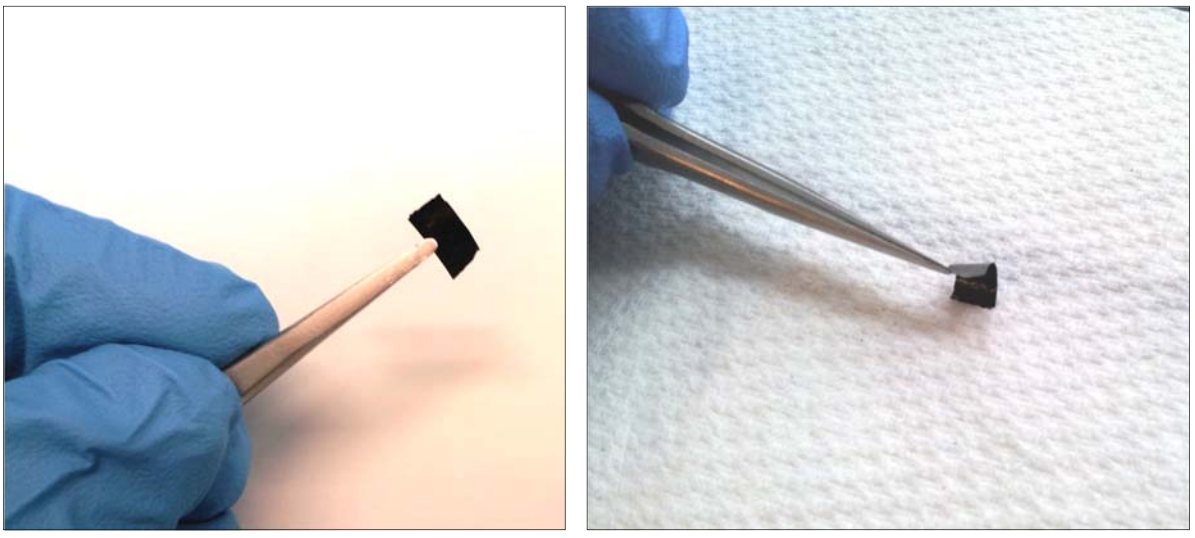

(a) (b)

Figure 10